ResearchGate

See discussions, stats, and author profiles for this publication at: https://www.researchgate.net/publication/44689270

High-Performance Single Crystal Organic Field-Effect Transistors Based on Two Dithiophene-Tetrathiafulvalene (DT-TTF) Polymorphs

ARTICLE *in* ADVANCED MATERIALS · OCTOBER 2010

Impact Factor: 17.49 · DOI: 10.1002/adma.201001446 · Source: PubMed

CITATIONS
47

READS
66

17 AUTHORS, INCLUDING:

Tomasz Marszalek
Max Planck Institute for Polymer Research
28 PUBLICATIONS **179** CITATIONS
SEE PROFILE

Jacek Ulanski
Lodz University of Technology
222 PUBLICATIONS **1,793** CITATIONS
SEE PROFILE

Jaume Veciana
Spanish National Research Council
981 PUBLICATIONS **12,167** CITATIONS
SEE PROFILE

Concepcio. Rovira
Spanish National Research Council
528 PUBLICATIONS **8,950** CITATIONS
SEE PROFILE

Available from: Jacek Ulanski
Retrieved on: 16 January 2016

High-Performance Single Crystal Organic Field-Effect Transistors Based on Two Dithiophene-Tetrathiafulvalene (DT-TTF) Polymorphs

By *Raphael Pfattner, Marta Mas-Torrent,* Ivano Bilotti, Aldo Brillante, Silvia Milita, Fabiola Liscio, Fabio Biscarini, Tomasz Marszalek, Jacek Ulanski, Andrzej Nosal, Maciej Gazicki-Lipman, Michael Leufgen, Georg Schmidt, Laurens W. Molenkamp, Vladimir Laukhin, Jaume Veciana,* and *Concepció Rovira**

Over the past years the use of organic semiconductors in field-effect transistors as an alternative to more traditional technologies based on inorganic semiconductors has been topic of numerous investigations.[1] Low cost production as a result of solution processability and large area coverage are some of the main issues in this field.[2] However, to study the intrinsic charge transport properties of organic semiconductors and to carry out correlation studies between crystal structure and device performance, single crystal devices are needed. The higher performance found in single crystal organic field-effect transistors (OFETs) compared to thin-film OFETs is related to the high molecular ordering and the absence of grain boundaries in the crystals.[3] High mobilities of the order of 10 $cm^2\ V^{-1}\ s^{-1}$ have been found for pentacene[4] and rubrene[5] single crystal-based devices, which, however, were prepared from vapor deposition techniques under strict controlled conditions and are often measured under oxygen and moisture free environments. Tetrathiafulvalenes (TTF) have also been shown to be promising organic semiconductors because of their high performance and processability.[6–14] In particular, solution-prepared single crystal OFETs based on dithiophene-tetrathiafulvalene (DT-TTF **Figure 1a**) and dibenzo-tetrathiafulvalene (DB-TTF) as active materials showed hole mobilities of up to 3.6 and 1.0 $cm^2\ V^{-1}\ s^{-1}$, respectively, under ambient conditions.[10,11] Some works focused on investigating OFETs based on TTF derivatives that exhibit different solid-state structures have evidenced the extremely high influence of the crystal structure on the transport properties.[12,13] Polymorphism also represents another crucial issue as it has been reported for the parent compound TTF[14] and for DB-TTF,[15] where up to four polymorphic modifications have been identified. In addition, all this complexity is further increased by the large number of device parameters that affect the final OFET performance. In this letter we report on OFETs based on solution-prepared DT-TTF single crystals, where a new polymorph, called hereafter β-DT-TTF, was found. This opened the opportunity to further study the charge transport and related device performance of OFETs based on one active material, but in different solid-state structures, and in distinct device architectures.

Long plate crystals of DT-TTF, namely the α-phase, can be easily prepared from solution employing a variety of solvents.[10,16] These crystals belong to the monoclinic system, space group $P2_1/a$, with two centrosymmetric molecules per unit cell.[17] The molecules arrange in a herringbone structure with the long axis tilted almost 20° to the *c*-axis and facing along *b*, the shortest crystal axis that corresponds to the stacking direction of the molecules and, thus, where the π–π interactions are maximized (Figure 1b). However, when DT-TTF crystallizes on surfaces (i.e., SiO_2 or Parylene C) from a solution of toluene or dichlorobenzene, crystals showing thin hexagonal-shaped platelets coexist with the clearly identified crystals of the α-phase (Figure 1**c**). Using an optical microscope equipped with a polarizer-analyzer the quality of the single crystals was proved. The crystallization of the material on the substrate never led to one unique phase.

[*] R. Pfattner, Dr. M. Mas-Torrent, Prof. V. Laukhin, Prof. J. Veciana, Prof. C. Rovira
Institut de Ciencia de Materials de Barcelona (ICMAB-CSIC)
Campus UAB, 08193 Bellaterra (Spain)
Networking Research Center on Bioengineering
Biomaterials and Nanomedicine (CIBER-BBN)
Bellaterra (Spain)
E-mail: mmas@icmab.es; cun@icmab.es
Prof. V. Laukhin
Institució Catalana de Recerca i Estudis Avançats (ICREA)
ICMAB-CSIC, 08193-Bellaterra (Spain)
Dr. I. Bilotti, Prof. A. Brillante
Dipartimento di Chimica Fisica e Inorganica
and INSTM-UdR Bologna
Universitá di Bologna
40136 Bologna (Italy)
Dr. S. Milita, Dr. F. Liscio
CNR- Instituto per la Microelettronica e Microsistemi (IMM)
40129 Bologna (Italy)
Prof. F. Biscarini
CNR- Instituto per lo Studio dei Materiali Nanostrutturati (ISMN)
40129 Bologna (Italy)
Dr. M. Leufgen, Dr. G. Schmidt, Prof. L. W. Molenkamp
Universität Würzburg
Physikalisches Institut (EP3)
Am Hubland, 97074 Würzburg (Germany)
T. Marszalek, Prof. J. Ulanski
Department of Molecular Physics
Technical University of Lodz
90–924 Lodz (Poland)
A. Nosal, Prof. M. Gazicki-Lipman
Institute of Mechanical Engineering
Technical University of Lodz
90–924 Lodz (Poland)

DOI: 10.1002/adma.201001446

© 2010 WILEY-VCH Verlag GmbH & Co. KGaA, Weinheim

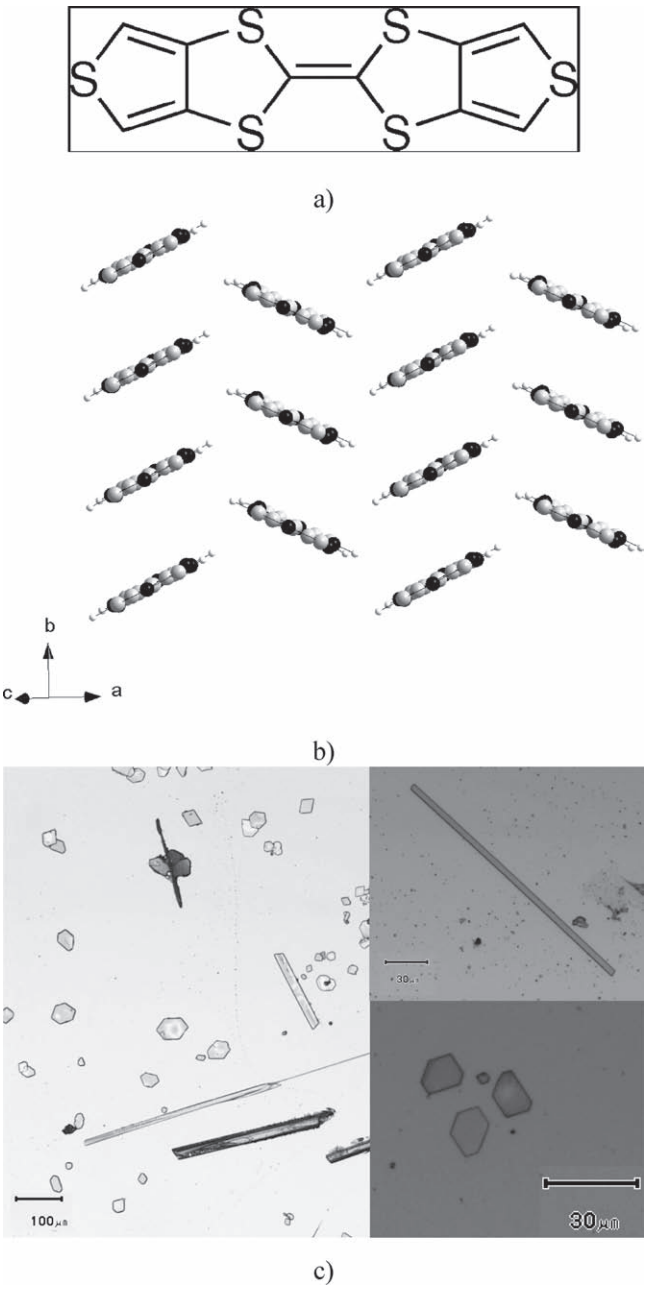

Figure 1. a) Molecular structure of DT-TTF. b) Crystal packing of the α-DT-TTF polymorph. c) Left: Solution prepared single crystals of DT-TTF on a Si/SiO_2 substrate. Two different polymorphs, that co-exist on the same substrate, can be clearly observed. Right: Optical microscope images of both the α-DT-TTF (top) and the β-DT-TTF (bottom) phases.

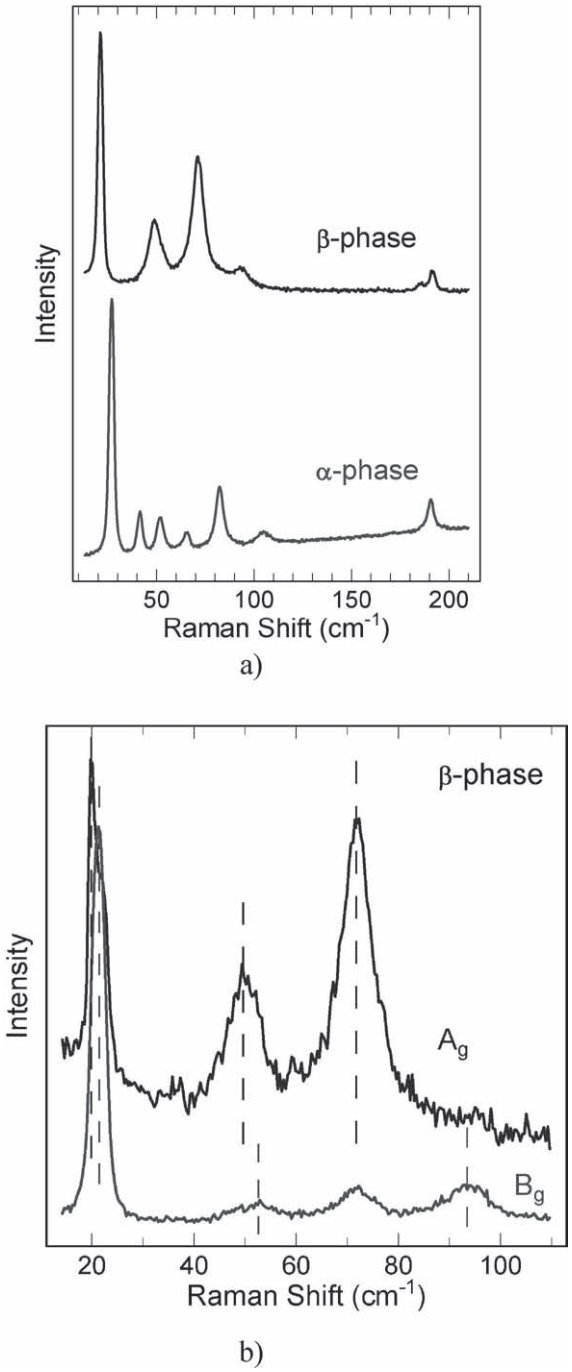

Figure 2. a) Lattice phonon Raman spectra of α-DT-TTF and β-DT-TTF single crystals. b) Polarized Raman spectra of the β-DT-TTF in the lattice phonon region. Upper and lower traces refer to (par-par) and (par-per) configurations and are identified as A_g and B_g, respectively.

However, by submitting the solution to ultrasound before drop casting, the amount of β-DT-TTF increased, whereas the α-phase was mostly obtained when small seed crystals were present. This indicates that, in the case of the α-phase, the crystallization probably starts in the solution and then the crystals fall onto the substrate, while the β-phase crystallizes directly on the substrate.

To verify the presence of two polymorphs with stable crystal structures at ambient conditions, we performed a lattice phonon Raman investigation,[18] which has proved to be a very powerful technique in identifying polymorphs of other semiconductors[15,19–22] both in the bulk crystals and in thin films. Indeed, the Raman spectra clearly confirmed that the two DT-TTF crystal morphologies correspond to two different polymorphic forms (**Figure 2a**). Since both polymorphs have been prepared as single crystals, Raman spectra could be studied in polarized light, yielding information on the symmetry assignment of

© 2010 WILEY-VCH Verlag GmbH & Co. KGaA, Weinheim

lattice phonons (see Supporting Information (SI) for polarized Raman data for the α-phase).

The polarized spectra for single crystals of the β-phase are complicated to interpret because its space group is unknown. However, some hints on its structure could be drawn from the analysis of the phonon spectra. The single crystal was placed on the stage of the spectrometer with its extinction directions either parallel (par) or perpendicular (perp) to the polarization directions of the incident laser radiation. This ensures that the principal crystal directions, i.e., those coincident with the diagonal elements of the refractive index matrix, can be properly aligned parallel (par-par) to the polarization directions of the scattered radiation or perpendicular (par-perp) to it. Theory shows[23] that, independently of the space group, total-symmetric modes are observed for the diagonal components (par-par), whereas non total-symmetric modes appear in some of the off-diagonal elements (par-perp). Results are shown in Figure 2b, where par-par and par-perp spectra are reported on the top and at the bottom, respectively. We observed, with the exception of a residual polarization at about 72 cm^{-1}, a total of six lattice phonons and a clear mutual exclusion between modes belonging to the par-par and par-perp geometrical configurations. This is consistent with a polarizability tensor of a centro-symmetric monoclinic group (space group C_{2h}^5) with two molecules per unit cell,[23] like the α-polymorph. We thus assign total-symmetric modes observed for the diagonal components (par-par) to the A_g symmetry, whereas non total-symmetric B_g modes appear in off-diagonal elements (par-perp).

Raman spectra were also performed in DT-TTF thin-films prepared by evaporation. We observed that in the films prepared on hydrophilic SiO_2 only the pure β-phase was present, whereas in the ones prepared on OTS (octadecyltrichlorosilane)-treated SiO_2 surfaces a very slight contamination of the α-phase was sometimes found (for more details regarding phase mixing see the SI). All these results suggest that the DT-TTF α-phase is the thermodynamically most stable structure and that the β-phase is only stable in a thin-film morphology, reminiscent of the γ-phase of DB-TTF.[15]

In order to gain further information on the crystal structure of β-DT-TTF, X-ray analysis of evaporated thin-films on hydrophilic SiO_2 and on OTS-treated SiO_2 surfaces was carried out (see SI for detailed X-ray data). The diffraction patterns recorded in specular geometry ($2\theta/\omega$ scan) exhibited only the presence of peaks related to a periodicity of 13.18 Å, which is slightly larger than the (001) spacing of the known α-phase (13.11 Å). This suggests that DT-TTF molecules assemble on the substrate surfaces with the long molecular axis aligned approximately parallel to the surface normal. 2D-Grazing incidence diffraction (GID) images (see SI) clearly indicate the fiber-like texture of the films, common for organic thin film systems, which have the main axis perpendicular to the sample surface, where the a^*b^* plane of the reciprocal unit cell lies parallel. Moreover, the unit cell of the β-phase could be determined by combining the analysis of the X-Ray measurements performed by GID (2D images and the high-resolution scans) and in out-of plane geometries. By assuming a monoclinic crystal structure, as suggested by Raman results, the positions of the experimental reflections could be reproduced by space group $P2_1/a$ and unit cell parameters a = 5.803 Å, b = 7.640 Å, c = 13.176 Å, and β = 90.828°, and V = 584 $Å^3$. The absence of $0k0$ and $h00$ reflections in the GID patterns indicates that the projection of the structure on the a^*b^* plane has a $p2gg$ symmetry, which corresponds to molecules arranged in a herringbone configuration. We should underline that this is not an unambiguous crystal structure able to reproduce the diffraction patterns, although it represents a physically reasonable solution.

Noticeably, the X-ray diffraction of DT-TTF single-crystal hexagonal-shaped platelets on SiO_2 suggests that they have the same β-phase structure determined for sublimated thin films.

It is worth highlighting here the importance of identifying different polymorphs, as well as their phase mixing, in materials for organic electronics, since boundaries between different phases produce an intrinsic source of disorder, with detrimental effects on the charge transport.[24]

In order to study the performance in OFETs, solution-prepared single crystals of both polymorphs were employed as active organic semiconductors in different device architectures. Besides the bottom-gate bottom-contact (BGBC) geometry, where gold was used as the source and drain electrodes, also a bottom-gate top-contact (BGTC) architecture, applying graphite paste as the source and drain electrodes, was used. Since the quality of the dielectric/semiconductor interface is crucial for achieving high device performance,[25] we also investigated the influence of two type of dielectrics, SiO_2 and Parylene C, on both device configurations.

Figure 3a shows an optical microscope image of one of the best performing OFETs based on β-DT-TTF, which was prepared using the organic insulator Parylene C as dielectric in a BGBC geometry. The hexagonal shape of the single crystal of β-DT-TTF, typical for this phase, is clearly observable. The channel width and length were found to be W = 450 µm and L = 80 µm, respectively. When sweeping the source–drain voltage in the output characteristics (Figure 3b), forwardly and reversely, hardly any hysteresis was observed. This indicates a low trapping level of charge carriers and it is evidence of the high quality of the interface between the organic single crystal and the dielectric. Low off-currents, in agreement with a low level of unintentional doping, and a good saturation behavior at the channel pinch-off were observed. A low threshold voltage (V_{TH} = 3.14 V) indicated again a low unintentional doping level of the device. The field-effect mobility, calculated in the saturation regime, gave a high mobility of 0.13 $cm^2\ V^{-1}\ s^{-1}$ (see transfer characteristics in Figure 3**c**).

One of the best performing devices based on a solution prepared α-DT-TTF single crystal is shown in the optical microscope image in **Figure 4a**. This device was prepared in a BGTC architecture, using a Si/SiO_2 substrate and drawing graphite source and drain electrodes. The corresponding output and transfer characteristics, showing textbook like behavior, are shown in Figures 4b,c. Channel width and length were measured to be W = 28 µm and L = 336 µm, respectively, for this device. The quality of the semiconductor/insulator interface is again reflected in the low hysteresis between forwardly and reversely swept source–drain voltages. A low threshold voltage (V_{TH} = −1.52 V) was also found for this device. In addition, the good saturation behavior and low off-currents are in accordance with the excellent device performance, which revealed a field-effect mobility as high as 0.63 $cm^2\ V^{-1}\ s^{-1}$, extracted in the saturation regime.

© 2010 WILEY-VCH Verlag GmbH & Co. KGaA, Weinheim

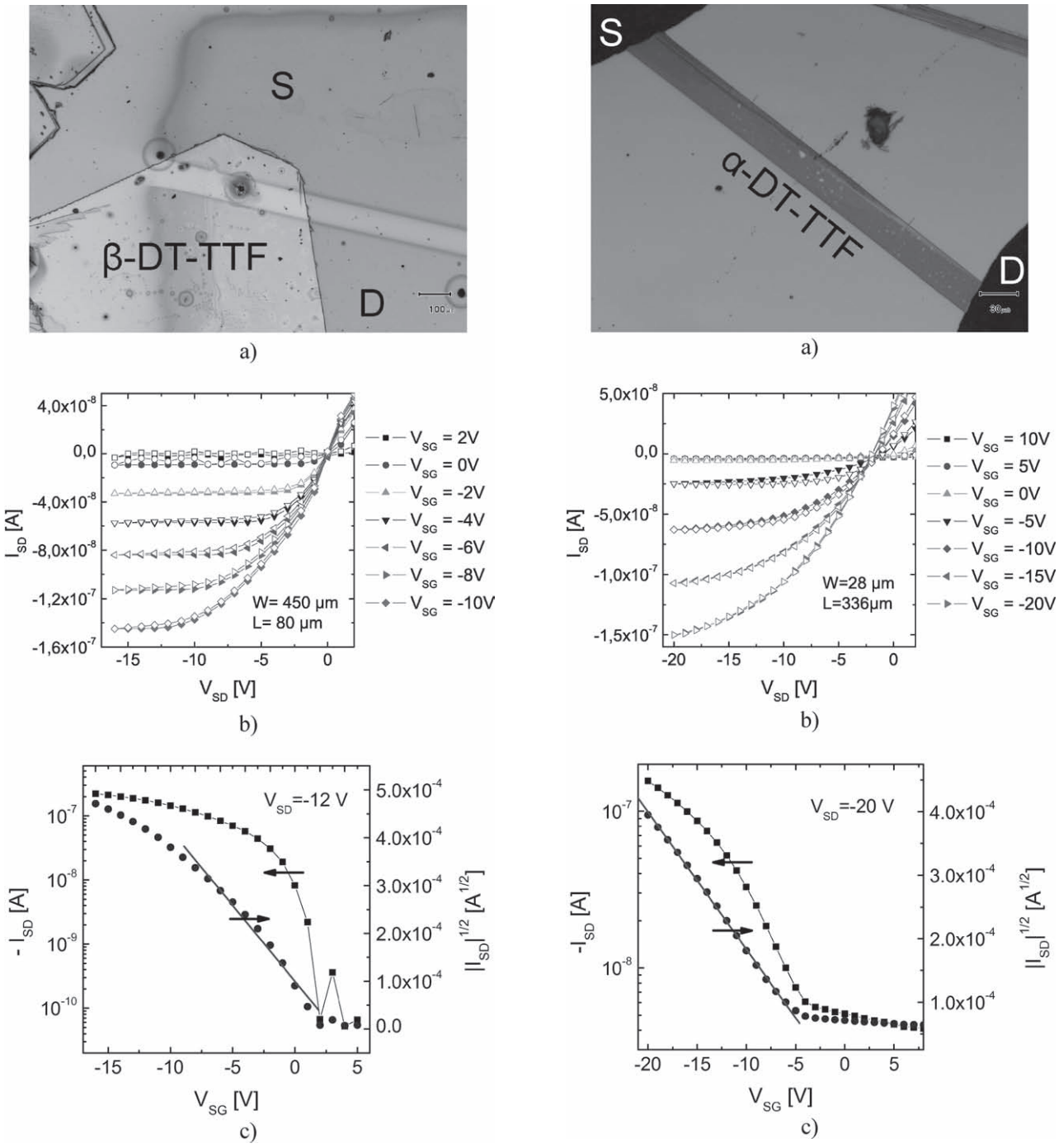

Figure 3. Single crystal OFET based on β-DT-TTF. a) Optical microscope image of the device with gold source (S) and drain (D) electrodes and Parylene C as dielectric. b) Output characteristics measured sweeping the source–drain voltage forwardly (closed symbols) and reversely (open symbols). Channel width and length of this device are 450 and 80 µm, respectively. c) Transfer characteristics and linear fit to extract field-effect mobility.

Figure 4. Single crystal OFET based on α-DT-TTF. a) Optical microscope image of the device with graphite source (S) and drain (D) electrodes and SiO_2 as dielectric. b) Output characteristics measured sweeping the source–drain voltage forwardly (closed symbols) and reversely (open symbols). Channel width and length of this device are 28 and 336 µm respectively. c) Transfer characteristics and linear fit to extract field-effect mobility.

In order to show an overview of the results obtained applying BGBC and BGTC architectures, the main OFET parameters are summarized in **Table 1** and **Table 2**, respectively. As mentioned before, in both configurations SiO_2 and Parylene C were used as the dielectric, while for the source–drain contacts gold was used in the BGBC geometry and graphite in the BGTC. Although comparisons have to be carried out in caution, we can easily see that the results achieved with the two different device configurations are very similar. Thus, we demonstrate that the utilization of graphite paste for fabricating source and drain

© 2010 WILEY-VCH Verlag GmbH & Co. KGaA, Weinheim

Table 1. DT-TTF OFETs based on a BGBC architecture with either SiO_2 or Parylene C as gate-dielectric and gold as source and drain electrodes. $\mu_{FE;SAT}$: field-effect mobility calculated in the saturation regime;[27,28] V_{TH}: Threshold voltage; I_{ON}/I_{OFF}: current on/off ratio.

	α-DT-TTF		β-DT-TTF	
Gate/dielectric	Si/SiO_2	Au/Parylene C	Si/SiO_2	Au/Parylene C
$\mu_{FE,SAT}$ [$cm^2 V^{-1} s^{-1}$]	0.57 ± 0.15	1.0 ± 0.3	0.15 ± 0.01	0.17 ± 0.03
V_{TH} [V]	8.1 ± 0.5	12.36	4.3 ± 5.5	2.9 ± 0.2
I_{ON}/I_{OFF}	~10^2	~10^2	~10^3	~10^4

Table 2. DT-TTF OFETs based on a BGTC architecture with either SiO_2 or Parylene C as gate-dielectric and graphite based source and drain electrodes. $\mu_{FE;SAT}$: field-effect mobility calculated in the saturation regime;[27,28] V_{TH} : Threshold voltage; I_{ON}/I_{OFF}: Current on/off ratio.

	α-DT-TTF		β-DT-TTF	
Gate/dielectric	Si/SiO_2	Au/Parylene C	Si/SiO_2	Au/Parylene C
$\mu_{FE,SAT}$ [$cm^2 V^{-1} s^{-1}$]	0.63 ± 0.04	1.18 ± 0.09	0.03 ± 0.01	0.16 ± 0.05
V_{TH} [V]	–0.1 ± 2.4	15.1 ± 1.2	9.4 ± 3.9	6.7 ± 1.1
I_{ON}/I_{OFF}	~10^3	~10^2	~10^2	~10^4

electrodes represents a useful alternative to gold electrodes. Another general conclusion that can be easily drawn is that all devices based on Parylene C as dielectric showed higher mobilities with respect to the corresponding OFETs fabricated on SiO_2, pointing out that the organic/organic interface between the semiconductor and the dielectric is more favorable.

Comparing the OFET results between the two polymorphs, the overall message is that the α-DT-TTF crystals show a higher field-effect mobility than the β-DT-TTF. When using SiO_2 as dielectric the difference in mobility is between two and four times, but with Parylene C the difference becomes more accentuated reaching mobility values of almost one order of magnitude higher for α-DT-TTF. Importantly, this observation agrees with the data obtained from X-ray and Raman analyses, which predict that although both polymorphs show a very similar monoclinic crystal structure, the distance between adjacent molecules along the stacking direction is larger for β-DT-TTF and, hence, the electronic coupling will be smaller.[26] We should note, though, that the high positive threshold voltages found for devices based on α-DT-TTF, especially when using Parylene C as a dielectric, are related to unintentional doping, which is not taken into account in the applied standard mobility calculations.[27,28] Also, the lower on/off current ratio observed in the devices prepared with α-DT-TTF can be attributed to the effective channel dimensions since the W/L ratio in OFETs based on long plate-shaped crystals is very low in comparison with devices with hexagonal platelets of β-DT-TTF.

Previously, we reported that the preparation on SiO_2 of DT-TTF films from solution using the zone-casting technique led to the formation of the α-phase.[29] Although lower than the single crystal devices, a remarkable performance with a maximum mobility of 0.17 $cm^2 V^{-1} s^{-1}$ was measured for OFETs prepared using these films by evaporating top Au source and drain electrodes. As mentioned before, evaporated films prepared on hydrophilic SiO_2 resulted in the formation of a pure β-phase, which gave us the opportunity to also investigate the influence of film polymorphism in the OFET performance. Following the same methodology, OFETs were also prepared with these films which gave a mobility of up to 0.068 $cm^2 V^{-1} s^{-1}$ (see the SI). These results are fully in agreement with the ones obtained with the single crystal devices, pointing out again the higher intrinsic mobility of the α-DT-TTF polymorph.

In summary, a new polymorph of DT-TTF, β-phase, has been found in single crystals prepared on a surface from solution and in evaporated thin films, and investigated by confocal Raman spectroscopy and X-ray diffraction analysis. The solution-processed single crystal OFET performance of both polymorphs, the already studied α-DT-TTF and the newly found β-DT-TTF, was tested in different device architectures. All the devices exhibited excellent performance. Of particular note is that all α-DT-TTF-based single crystal and thin film OFETs showed a higher mobility than the β-DT-TTF OFETs. This result is in agreement with the crystallographic studies, which revealed that both phases show a similar crystal structure, but distances between neighboring molecules are larger for β-DT-TTF single crystals. To establish a correlation between solid-state structure and device properties is crucial in order to further understand the transport phenomena. Moreover, if organic devices are going to be implemented for commercial use, it will be imperative to be aware of the control of polymorphism in organic semiconductors.

Experimental Section

DT-TTF was synthesized as previously described.[17]

Single crystals of DT-TTF on surfaces were grown from solution by drop casting 50 μL and allowing the solvent (e.g., chlorobenzene or toluene, conc. = 1 mg mL^{-1}) to evaporate slowly as previously described.[9] In order to reduce unintentional doping the crystallization process was carried out under darkness and reduced ambient humidity at room temperature.

Thin films of DT-TTF were thermally evaporated onto SiO_2 under vacuum (10^{-2} torr) at $T = 190°C$.

Optical Microscopy: Optical microscope images were taken with an Olympus BX51 that included a polarizer and analyzer for the analysis of crystalline materials.

Raman Spectroscopy: DT-TTF single crystals were placed on the stage of an optical microscope (Olympus BX40) interfaced to a Jobin Yvon T64000 Raman spectrometer, with 50 x or 100 x objectives, which allowed a spatial resolution of about 1 μm and a theoretical field depth that ranged from about 7 to 25 μm. Spectra were recorded spanning the region 10–2000 cm^{-1}, with particular attention to the low wavenumber region of the lattice phonons (10–150 cm^{-1}). A krypton laser tuned to 647.1 nm exhibited an excitation energy sufficiently low to avoid background fluorescence from the sample. The actual power on the sample was reduced (less than 1 mW) with a neutral filter, whose optical density was selected in each experiment to prevent crystal damage. Molecular identity was checked by simultaneously detecting the intramolecular vibrations of the skeletal modes of DT-TTF.

X-Ray Characterization: X-ray diffraction measurements (in both out-of-plane and GI in-plane geometries) were carried out with a diffractometer equipped by a rotating anode source (model SmartLab of Rigaku Company). A focus line X-ray beam (Cu Kα) was collimated by a parabolic graded multilayer mirror placed in front of the sample and a double slit was mounted before the detector to achieve the required angular resolution. High-resolution GID in-plane measurements were

© 2010 WILEY-VCH Verlag GmbH & Co. KGaA, Weinheim

performed at the ID10B beamline at ESRF (Grenoble, France) by using a monochromatic beam of 1.5515 Å.

GID 2D images were collected at the XRD1 beam line at the ELETTRA (Trieste, Italy) facility by using a monochromatic beam of 1.5498 Å. The incident angle was about 1 deg and the 2D CCD camera was placed normal to the incident beam direction at 138 mm to record the reflection pattern.

OFET Devices: Si/SiO_2 substrates were from SiMat wafers. The Au/Parylene substrates were prepared as described in the following. On a previously cleaned glass substrate, 10 µm of Parylene C was deposited. Afterwards a 120 nm thick Au layer used as a gate was thermally evaporated on top. Finally, a second 1 µm thick Parylene C layer was applied and used as a gate dielectric. For the BGBC configuration, the source–drain Au electrodes were fabricated by evaporation using a shadow mask on top of the dielectric. In the case of the BGTC architecture, the source and drain electrodes (graphite paste) were drawn on top of the single crystals. The electrical characterization was done using a two channel Keithley Source Meter 2612. A specially adapted Matlab program, using instrument control toolbox 2.5, was used to remotely control the device for OFET measurements. All devices were connected and measured under darkness and ambient conditions using micro manipulators within a Süss Micro Tech Probe Station (T = 28 °C, relative humidity = 40–50%). The field-effect mobility was calculated in the saturation regime using **Equation 1**. By plotting the square root of the saturation current ($I_{SD,SAT}$) versus the gate voltage and performing a linear fit the field-effect mobility (μ_{SAT}) and the threshold voltage (V_{TH}) can be extracted.[27,28]

$$\mu_{SAT} = \frac{2L}{WC_i}\left(\frac{\partial\sqrt{I_{SD,SAT}}}{\partial V_{SG}}\right)^2 \quad (1)$$

where C_i is the insulator capacitance per unit area, and W and L are the width and length of the crystal between the electrodes, respectively.

Supporting Information

Supporting Information is available from the Wiley Online Library or from the author.

Acknowledgements

The authors thank the EU Large Project One-P (FP7-NMP-2007–212311), Marie Curie Est FuMaSSEC, the Networking Research Center on Bioengineering, Biomaterials, and Nanomedicine (CIBER-BBN), the DGI (Spain, CTQ2006-06333/BQU), Generalitat de Catalunya 2009SGR158, and the bilateral project Poland-Spain (MAT2006–28191-E and HISZPANIA/140/2006).

Received: April 20, 2010
Revised: May 6, 2010
Published online: June 18, 2010

[1] a) M. Mas-Torrent, C. Rovira, *Chem. Soc. Rev.* **2008**, *37*, 827; b) J. Zaumseil, H. Sirringhaus, *Chem. Rev.* **2007**, *107*, 1296; c) D. R. Gamota, P. Brazis, X. Kalyanasundaram, J. Zhang, Printed Organic and Molecular Electronics, *Kluwer Academic Publishers*, New York, **2004**; d) L. L. Chua, J. Zaumseil, J. F. Chang, E. C. W. Ou, P. K. H. Ho, H. Sirringhaus, R. H. Friend, *Nature* **2005**, *434*, 194.
[2] S. R. Forrest, *Nature* **2004**, *428*, 911.
[3] W. Warta, N. Karl, *Phys. Rev. B* **1985**, *32*, 1172.
[4] Luke B. Roberson, J. Kowalik, L. M. Tolbert, C. Kloc, R. Zeis, X. Chi, R. Fleming, C. Wilkins, *J. Am. Chem. Soc.* **2005**, *127*, 3069.
[5] V. Podzorov, S. E. Sysoev, E. Loginova, V. M. Pudalov, M. E. Gershenson, *Appl. Phys. Lett.* **2003**, *83*, 3504.
[6] M. Mas-Torrent, C. Rovira, *J. Mater. Chem.* **2006**, *16*, 433.
[7] M. –S. Nam, A. Ardavan, R. J. Cava, P. M. Chaikin, *Appl. Phys. Lett.* **2003**, *83*, 4782.
[8] a) Y. Takahashi, T. Hasegawa, S. Horiuchi, R. Kumai, Y. Tokura, G. Saito, *Chem. Mater.* **2007**, *19*, 6382; b) Naraso, J. Nishida, D. Kumaki, S. Tokito, Y. Yamashita, *J. Am. Chem. Soc.* **2006**, *128*, 9598; c) X. K. Gao, Y. Wang, X. D. Yang, Y. Q. Liu, W. F. Qiu, W. P. Wu, H. J. Zhang, T. Qi, Y. Liu, K. Lu, C. Y. Du, Z. G. Shuai, G. Yu, D. B. Zhu, *Adv. Mater.* **2007**, *19*, 3037.
[9] P. Miskiewicz, M. Mas-Torrent, J. Jung, S. Kotarba, I. Glowacki, E. Gomar-Nadal, D. B. Amabilino, C. Rovira, J. Veciana, B. Krause, D. Carbone, J. Ulanski, *Chem. Mater.* **2006**, *18*, 4724.
[10] a) M. Mas-Torrent, M. Durkut, P. Hadley, X. Ribas, C. Rovira, *J. Am. Chem. Soc.* **2004**, *126*, 984; b) M. Leufgen, O. Rost, C. Gould, G. Schmidt, J. Geurts, L. W. Molenkamp, N. S. Oxtoby, M. Mas-Torrent, N. Crivillers, J. Veciana, C. Rovira, *Organic Electronics* **2008**, *9*, 1101.
[11] M. Mas-Torrent, P. Hadley, S. T. Bromley, N. Crivillers, J. Veciana, C. Rovira, *Appl. Phys. Lett.* **2005**, *86*, 012 110.
[12] M. Mas-Torrent, P. Hadley, S. T. Bromley, X. Ribas, J. Tarrés, M. Mas, E. Molins, J. Veciana, C. Rovira, *J. Am. Chem. Soc.* **2004**, *126*, 8546.
[13] B. Noda, H. Wada, K. Shibata, T. Yoshino, M. Katsuhara, I. Aoyagi, T. Mori, T. Taguchi, T. Kambayashi, K. Ishikawa, H. Takezoe, *Nanotechnology* **2007**, *18*, 424 009
[14] H. Jiang, X. Yang, Z. Cui, Y. Liu, H. Li, W. Hu, Y. Liu, D. Zhu, *Appl. Phys. Lett.* **2007**, *91*, 123 505.
[15] A. Brillante, I. Bilotti, R. G. Della Valle, E. Venuti, S. Milita, C. Dionigi, F. Borgatti, A. N. Lazar, F. Biscarini, M. Mas-Torrent, N. Oxtoby, N. Crivillers, J. Veciana, C. Rovira, M. Leufgen, G. Schmidt, L. W. Molenkamp, *CrystEngComm*. **2008**, *10*, 1899.
[16] M. Mas-Torrent, P. Hadley, X. Ribas, C. Rovira, *Synthetic Metals* **2004**, *146*, 265.
[17] The unit cell parameters of the α-DT-TTF were found to be: a = 10.906 Å, b = 3.991 Å, c = 14.030 Å, β = 110.82° and V = 570.792 Å^3. C. Rovira, J. Veciana, N Santaló, Judit Tarr s, J. Cirujeda, E. Molins, J. Llorca, E. Espinosa, *J. Org. Chem.* **1994**, *59*, 3307.
[18] A. Brillante, I. Bilotti, R. G. Della Valle, E. Venuti, A. Girlando, *CrystEngComm*. **2008**, *10*, 937.
[19] A. Brillante, I. Bilotti, R. G. Della Valle, E. Venuti, M. Masino, A. Girlando, *Adv. Mater.* **2005**, *17*, 2549.
[20] E. Venuti, R. G. Della Valle, L. Farina, A. Brillante, M. Masino, A. Girlando, *Phys. Rev. B* **2004**, *70*, 104 106.
[21] A. Brillante, I. Bilotti, F. Biscarini, R. G. Della Valle, E. Venuti, *Chem. Phys.* **2006**, *328*, 125.
[22] A. Brillante, I. Bilotti, C. Albonetti, J-F. Moulin, P. Stoliar, F. Biscarini, D. M. de Leeuw, *Adv. Funct. Mater.* **2007**, *17*, 3119.
[23] G. Turrell, *Infrared and Raman Spectra of Crystals*, Academic Press, London, **1972**.
[24] H. Sirringhaus, *Adv. Mater.* **2009**, *21*, 3859.
[25] G. Horowitz, *Adv. Func. Mater.*, **2003**, *13*, 53.
[26] J. Cornil, J.-L. Brédas, J. Zaumseil, H. Sirringhaus, *Adv. Mater.*, **2007**, *19*, 1791.
[27] G. Horowitz, R. Hajlaoui, H. Bouchriha, R. Bourguiga, M. Hajlaoui, *Adv. Mater.* **1998**, *10*, 923.
[28] E. J. Meijer, C. Tanase, P. W. M. Blom, E. van Veenendaal, B.-H. Huisman, D. M. de Leeuw, T. M. Klapwijk, *Appl. Phys. Lett.* **2002**, *80*, 3838.
[29] M. Mas-Torrent, S. Masirek, P. Hadley, N. Crivillers, N. S. Oxtoby, P. Reuter, J. Veciana, C. Rovira, A. Tracz, *Org. Electron.* **2008**, *9*, 143.

© 2010 WILEY-VCH Verlag GmbH & Co. KGaA, Weinheim